HEFAT2014
10th International Conference on Heat Transfer, Fluid Mechanics and Thermodynamics
14 – 26 July 2014
Orlando, Florida

PARAMETRIC ANALYSIS OF THE HEAT TRANSFER IN IMPIMGING JETS

Fernandes C. A., Loureiro J.B.R.* and Silva Freire A. P.
*Author for correspondence
Mechanical Engineering Program,
Federal University of Rio de Janeiro,
C.P. 68503, 21941-972,Brazil,
E-mail: jbrloureiro@mecanica.coppe.ufrj.br

ABSTRACT

The paper shows how a phenomenological model can be constructed to develop a simulator that furnishes the dynamic and thermal properties of impinging jets in real time. The presented correlations cover a large range of flow conditions, are based on eleven different experimental data sets and furnish predictions for the local pressure distribution, mean velocity distribution, wall shear stress, temperature distribution and Nusselt number. The analysis considers that the flow properties can be determined in terms of gross parameters like the free-jet momentum flux, the free-jet heat flux per unit length and the wall heat flux.

INTRODUCTION

The simulation of industrial flows in real time provides obvious advantages for the implementation of control and automation systems in desired applications. One major problem, however, is the inherent difficulty in solving the Navier-Stokes equations. The non-linear and multi-scale character of high-Reynolds number flows makes any attempt at resolving the smallest dynamically important scales through direct numerical simulation an extremely difficult affair due to the very fine meshes and time steps that are required. In fact, even numerical approaches that resort to averaged equations and closure modelling are rendered impractical.

Unfortunately, many problems of interest involve fluids with small viscosities and large velocities, so that turbulence effects are frequently present in their fullness and complexity. As an alternative to the absence of analytical solutions or to very expensive and sophisticated numerical schemes, experimental methods of investigation together with parametric analyses can many times define simple working rules and predictive mathematical relations. Of course, to some analyses this approach may not rely on formal derivations based on the first principles so that results must be interpreted with much caution. However, in many instances simple experimental facts can be used to construct general laws expressed in terms of parameters that reflect the main effects of the phenomenon under consideration. For example, phenomenological models for the turbulent boundary layer and the wall jet have been introduced by Sreenivasan [1] and Narasimha [2] respectively.

NOMENCLATURE

A, A_1, A_2	Parameters in velocity law of the wall.
B, B_1, B_2	Parameters in temperature law of the wall.
C_1, C_2	Parameters in power-law expressions.
c_p	Specific heat.
D_1, D_2	Parameters in power-law expressions.
D	Nozzle diameter.
H	Nozzle-to-plate distance.
k	Thermal conductivity.
n_1, n_2	Parameters in power-law expressions.
m_1, m_2	Parameters in power-law expressions.
M_j	Jet momentum flux ($=DU_j^2$).
N_u	Nusselt number ($=hD/k$).
P	Pressure.
P_r	Prandtl number ($=\nu/\alpha$).
q_j	Free-jet heat ux per unit length ($=\rho c_p D U_j T_j$)
q_w	Wall heat flux.
r	Radial distance.
R_e	Reynolds number ($(DM_j)^{1/2}/\nu$).
S_1, S_2	Parameters in the free-jet far-field solution.
T_j	Free-jet temperature.
T_w	Wall temperature.
U, u	Longitudinal velocity component.
u_τ	Friction velocity.
x,y	Flow cartesian coordinates
$y_{0.5}$	Position of the half-velocity.

Greek symbols

α	Thermal diffusivity ($= k/(\rho c_p)$).
$\beta,\gamma,\sigma,\lambda,\zeta$	Parameters in Weibull distribution.
χ	von Karman's constant (=0.4).
χ_t	von Karman's constant, temperature profile (=0.44).
μ	Absolut viscosity.
μ	Mean value.
ν	Kinematic viscosity.
ρ	Density.
σ	Standard deviation.
τ	Shear stress.
ζ	r/D.

Subscripts

min	Local minimum.
max	Local maximum.
o	External flow conditions.
w	Wall condition.

One problem that is very difficult to treat both from the theoretical and numerical points of view, but yet has great practical relevance is that of an impinging jet onto a flat wall. The high heat and mass transfer characteristics of impinging jets have stimulated a voluminous bibliography on experimental, theoretical and numerical aspects of the problem which – in some ways expectedly – has not succeeded in clarifying some important issues. For example, some debate still persists in relation to the appearance of a second peak in the radial distribution of Nusselt number for some combinations of flow conditions [3]. The adequacy of turbulence models and near-wall approaches is also a subject of considerable dispute as argued by Pulat et al. [4].

The purpose of the present note is to discuss the implementation of a phenomenological simulator that can be run on real-time for the prediction of the dynamical and thermal properties of impinging jets. The approach is based on the recent arguments of Loureiro and Silva Freire [5] for the flow dynamics, together with some newly proposed expressions for the thermal properties. The new expressions are based on eleven [5, 6, 7, 8, 9, 10, 11, 12, 13, 14, 15] different sets of experimental data and furnish predictions for the local pressure distribution, mean velocity distribution, wall shear stress, temperature distribution and Nusselt number.

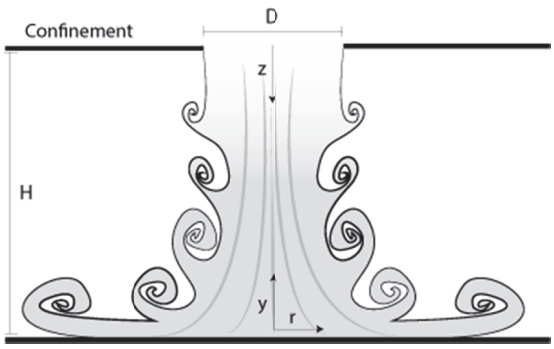

Figure 1 Schematic drawing of an impinging jet.

The analysis follows the approach introduced by Narasimha et al. [2] and considers that the flow properties can be determined in terms of gross parameters like the jet momentum flux (= DU_j^2), the free-jet heat flux per unit length (q_j) and the wall heat flux (q_w). The existence of near wall logarithmic regions for the velocity and temperature fields is also considered as presumed by Ozdemir and Whitelaw [16], Guerra et al. [9] and Loureiro and Silva Freire [5].

SIMILARITY ANALYSIS

The complex configuration of an impinging jet has been illustrated in the visualization study of Popiel and Trass [17] (see Fig. 1 for an schematic drawing). The existence of large-scale ordered structures is evident and determines much of the flow properties, as also explained by the LES simulations of Uddin et al. [3]. The evolution and breakdown of the jet ring vortices is further discussed in the LES investigation of Hadziabdi and Hanjalic [18].

Of course, analytical methods for the description of turbulent impinging jets cannot find solutions for the complete equations of motion, capable of describing the flow properties down to the smallest spatial and temporal scales. Rather, they seek approximate solutions based on the averaged equations. The solution procedure normally divides the flow into four regions. This division changes slightly from author to author. Poreh et al. [6] identifies four regions: the free-jet transition region, the free-jet region, the deflection zone and the radial wall jet. The classification of Phares et al. [19] divides the flow into the free jet region (consisting of near-field and far-field regions), the inviscid impingement region, the impingement boundary layer and the wall jet region. Of course, both pictures of the flow can be merged provided the deflection zone of Poreh et al. [6] is seen as a combination of the inviscid impingement region and the impingement boundary layer.

In their analytical approach to problem solution, Phares et al. [19] propose inviscid and boundary layer solutions to determine the wall shear stress in the small region of flow located just above the impingement plane. Poreh et al. [6] concentrated their analysis in the region of radial wall jet. The present developments deal with the free jet far-field region and the wall jet region. Poreh et al. [6] applied an integral method to the boundary layer equation and similarity arguments to arrive at a power-law relation between the radial position and the location and the magnitude of the maximum wall jet velocity.

Velocity Field

Free jet

A jet issuing from a nozzle consists of a potential core that owing to turbulence becomes partly mixed with the surrounding fluid. As a result, the jet spreads out, its velocity decreases, but the total momentum is conserved [20]. For distances over six nozzle diameters, the thin layer approximation together with Prandtl's eddy viscosity hypothesis can be used to obtain a similarity solution.

The far-field solution proposed by Schlichting [20] can be cast as

$$U_j(r,z) = S_1 \frac{K_S}{\varepsilon_0}\frac{1}{z}\left(1+\frac{1}{4}\eta(r,z)^2\right)^{-2}, \tag{1}$$

where

$$\eta(r,z) = S_2 \frac{1}{0.0161}\frac{r}{z}, \tag{2}$$

z is the axis oriented downstream along the jet axis, r is the radial direction, D is the nozzle diameter, and the following relations apply

$$S_1 = \frac{3}{8\pi}, \quad S_2 = \frac{1}{4}\left(\frac{3}{\pi}\right)^{1/2}, \tag{3a}$$

$$K_s = \frac{\pi D^2}{4}U_j^2, \qquad \varepsilon_0 = 0.0161 K_S^{1/2}. \tag{3b}$$

The pressure over an impinging wall can then be obtained by the simple consideration,

$$p(r) = \frac{1}{2}\rho U_j^2(r,H), \tag{4}$$

where H is the wall distance from the nozzle.

Wall jet

Regarding the velocity field, Phares et al. [19] proposed complete analytical solutions for the inviscid impingement region and the impingement boundary layer. In the wall jet region, however, predictions of the wall shear stress were provided by the empirical expression of Poreh et al. [6].

The wall jet region of an impinging jet was studied by Loureiro and Silva Freire [5] experimentally through Laser Doppler Anemometry and theoretically through the parametric approach suggested by Narasimha et al. [2]. The latter authors propose that at sufficiently large distances downstream of the issuing nozzle the flow dynamics is governed by the total momentum flux at the jet exit (M_j) and viscosity.

A further proposition by Ozdemir and Whitelaw [16] suggests that a Weibull distribution, given by Eq. (5) can be used to represent the global features of the mean velocity profile with $\gamma = 1.32$ and $\beta = 0.73$ and $y_{0.5} = y_{max}/0.2495$, so that

$$\frac{U}{U_{\max}} = \frac{\gamma}{\beta}\left(\frac{y/y_{0.5}}{\beta}\right)^{\gamma-1}\exp\left(-\left(\frac{y/y_{0.5}}{\beta}\right)^{\gamma}\right). \tag{5}$$

Ozdemir and Whitelaw [16] have also shown that near the wall a logarithmic velocity profile is observed with a level, A, that obeys a scaling law based on the stream-wise evolution of the flow characterized by its maximum velocity, U_{max}. Thus, according to Ozdemir and Whitelaw [16] the nozzle diameter is an inappropriate reference scaling.

To describe the logarithmic velocity profile, Ozdemir and Whitelaw [16] proposed an expression of the form:

$$\frac{u}{u_\tau} = \frac{1}{\chi}\ln\left(\frac{yu_\tau}{\nu}\right) + A, \tag{6}$$

with

$$A = A_1\frac{U_{\max}}{u_\tau} - A_2, \tag{7}$$

where $\chi = 0.4$, u_τ denotes the friction velocity and A_1 (= 0.962 [5]) and A_2 (= –8.987 [5]) are constants.

The analysis of Loureiro and Silva Freire [5] has shown that the following parametric relations apply in the wall region of an impinging jet,

$$\frac{U_{\max}\nu}{M_j} = C_1 R_e\frac{D}{H}\left(\frac{rM_j}{\nu^2}\right)^{m_1}, \tag{8}$$

$$\frac{y_{\max}M_j}{\nu^2} = C_2\left(\frac{rM_j}{\nu^2}\right)^{m_2}, \tag{9}$$

where C_1, m_1, C_2 and m_2 must be experimentally determined.

Given Eq. (9), the quantity $y_{0.5}$ can be determined from Eq. (5).

To determine the friction velocity, Eq. (5) can be solved at say, the point $y_c = 0.8y_{max}$ to give U_c. The pair (y_c, U_c) can then be substituted into Eq. (6) to find u_τ.

Temperature Field

We propose that the heat transfer problem is governed by parameters q_j (=$\rho c_p D U_j T_j$, jet heat flux per unit length) and q_w (= wall heat flux) and that the following relation holds

$$\frac{(T_w - T_j)k}{q_j} = D_1\frac{1}{R_e P_r}\frac{r}{D}\left(\frac{rq_w}{q_j}\right)^{n_1}, \tag{10}$$

where $R_e = (DM_j)^{1/2}/\nu$, $P_r = \nu/\alpha$.

Hence, given the flow dynamics and the wall heat flux, T_w can be found directly from Eq. (10).

Most authors present their thermal data in terms of the Nusselt number ($N_u = hD/k$, $h = q_w/(T_w - T_j)$). It follows immediately from Eq. (10) that

$$N_u = D_1^{-1}R_e P_r\frac{D}{r}\left(\frac{Dq_w}{q_j}\right)\left(\frac{q_j}{rq_w}\right)^{n_1}. \tag{11}$$

Guerra et al. [9] have shown that the inner temperature profile follows a logarithmic solution,

$$\frac{T_w - T}{t_\tau} = \frac{1}{\chi_t}\ln\left(\frac{yu_\tau}{\nu}\right) + B, \tag{12}$$

with

$$B = B_1\left(\frac{T_w - T_{\min}}{t_\tau}\right) - B_2, \tag{13}$$

where $B_1 = 1.031$ and $B_2 = -25.869$.

In the above equation, t_τ is the friction temperature (= $q_w/(\rho c_p u_\tau)$), u_τ is the friction velocity (=$(\tau_w/\rho)^{1/2}$) and $\chi_t = 0.44$.

The data of Guerra et al. [9] also suggest that the temperature profile follows a modified Weibull distribution,

$$\frac{T_w - T}{T_w - T_{\min}} = \frac{\sigma}{\lambda}\left(\frac{y/y_{0.5}}{\lambda}\right)^{\sigma-1}\exp\left(-\left(\frac{y/y_{0.5}}{\lambda}\right)^{\sigma}\right) + \varsigma\left(\frac{y/y_{0.5}}{\lambda}\right)^{\frac{1-\varsigma}{\sigma}}, \tag{14}$$

where, T_w = wall temperature, T_{min} = temperature minimum in temperature profile, y_{min} = height of minimum temperature, σ, γ and ζ must be determined form the experiments, and the last exponential term has been added since as $y \to \infty$, $T \to T_j$.

The position of y_{min} is here considered to be given by

$$\frac{y_{\min}q_w}{q_j} = D_2\left(\frac{rq_w}{q_j}\right)^{n_2}, \tag{15}$$

where D_2 is constant.

With Eqs. (12) and (15), T_{min} can be determined. For example, consider that Eq. (12) holds near to the point of minimum temperature so that it can be evaluated at y_{min} to yield T_{min}.

RESULTS

Most data in literature are presented in terms of parameters encapsulated in non-dimensional groups. The heat transfer to impinging jets is normally reported in terms of the Nusselt number. While in most situations this practice allows comparisons between experiments to be a straightforward affair, sometimes it may also make difficult the recovery of primitive parameters for the validation of alternative theories. Most works do not report the minimum mean statistics of the velocity and temperature fields. For example, local temperature profiles were only found in one reference. Also, some simple, but crucial, information is often left out of publications; many works do not report the wall heat flux or the free-jet temperature.

To characterize the flow dynamics, five sets of experimental results were used [5, 6, 7, 8, 9]. The velocity flow conditions are shown in Table 1. Data for both confined and unconfined flows for several *H/D* rates were considered.

Table 1 Velocity flow conditions.

Work	R_e	D(mm)	*H/D*	Confinement	m_1
[7]	18,800	13,3	2	No	–0.94
[9]	35,000	43,5	2	Yes	–1.05
[5]	47,100	43,5	2	Yes	–0.99
[6]	161,000	50,8	12	No	–1.09
[6]	196,000	50,8	12	No	–1.10
[8]	23,000	3,18	4	Yes	–1.08

The adequacy of a Weibull profile for the description of the mean velocity profile in the wall region is demonstrated in Fig. 2.

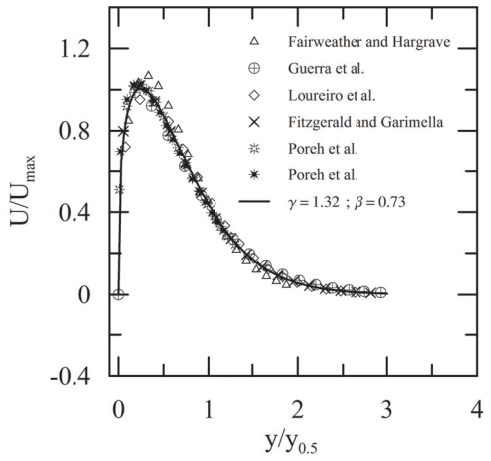

Figure 2 Weibull distribution for the mean velocity profile

The behaviour of U_{max} is shown in Fig. 3, where $m_1 = -1$ and $C_1 = 2.71$. To find m_1 and C_1 every velocity profile was initially plotted in log-log coordinates. Next, a best fit was chosen for every profile by searching for the maximum coefficient of determination, R-squared. Other statistical parameters were also observed, the residual sum of squares and the residual mean square. Normally, a coefficient of determination superior to 0.99 was obtained.

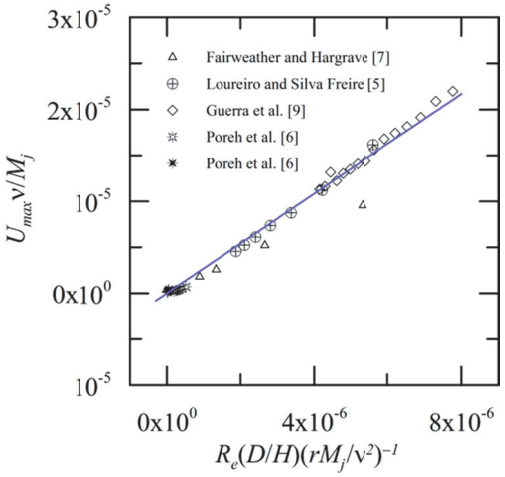

Figure 3 Dependence of U_{max} with the radial distance.

The values of m_1 ranged (see Table 1) from –0.94 to –1.1 with the average $\mu_{m1} = -1.02$ and the standard deviation $\sigma_{m1} = 0.057$. Here, we have fixed $m_1 = -1$ (Fig. 3). With m_1 chosen, a fit was applied to all data resulting in the final value of $C_1 = 2.71$, with residual mean square of 9.34×10^{-13}.

The determination of y_{max} is shown in Fig. 4. The exponent m_2 varied between 0.91 and 1.2 with $\mu_{m2} = 0.985$ and $\sigma_{m2} = 0.091$. Once m_2 was fixed equal to unity, the value of C_2 was determined as 0.0148, with residual mean square of 0.0023.

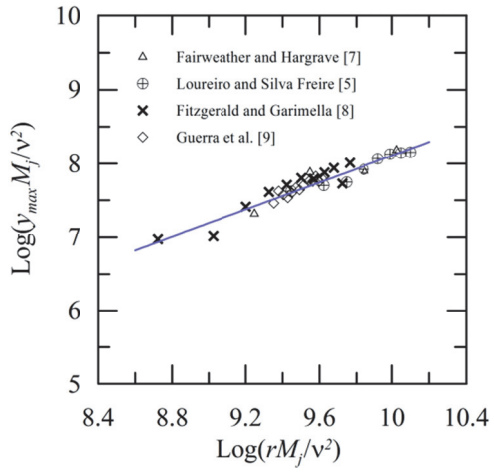

Figure 4 Dependence of y_{max} with the radial distance.

Temperature profiles are seldom presented in experimental or numerical works. However, they are important to characterize T_{min} and test Eq. (14). To validate Eqs. (14) and (15) we used the only set of experimental data that could be found in literature, the data of Guerra et al. [9]. The agreement with the proposed Weibull distribution, Eq. (14), is shown in Fig. 5 with $\sigma = 1.16$, $\lambda = 1.01$ and $\zeta = 0.46$.

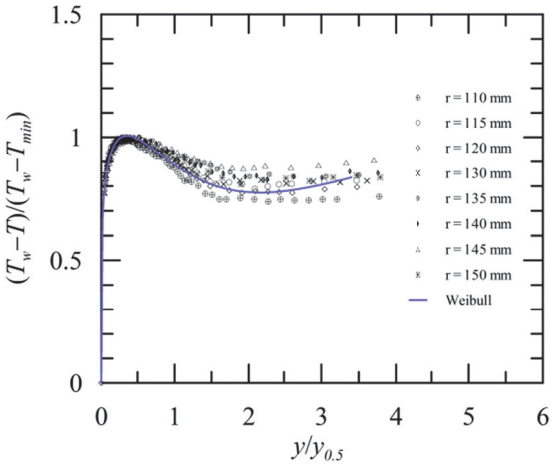

Figure 5 Weibull distribution for the radial mean temperature profiles of Guerra et al. [9].

The wall distance where the temperature profile reaches its minimum value is predicted through Eq. (15). The radial distribution of y_{min} is shown in Fig. 6, with $D_2 = 39527.1$ and $n_2 = 2.63$.

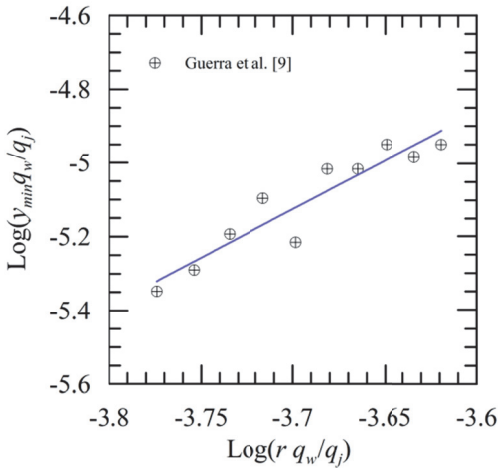

Figure 6 Radial distribution of the location of minimum temperature of the flow according to the data of Guerra et al. [9].

To validate the wall temperature parametrization, Eq. (10), we use the data sets of Guerra et al. [9], San et al. [11], San et al. [12], Huang et al. [13], Fenot et al. [14] and Ozmen et al. [15]. Data for both confined and unconfined flows and for several *H/D* rates were considered. The general experimental conditions are shown in Table 2.

Table 2 Reference data for the temperature field analysis.

Work	R_e	D(mm)	H/D	Confinement	n_1
[9]	35,000	43.5	2	Yes	–0.48
[11]	10,000	3	4	Yes	–0.50
[11]	20,000	3	4	Yes	–0.50
[11]	30,000	3	4	Yes	–0.51
[11]	10,000	10	4	Yes	–0.74
[11]	20,000	10	4	Yes	–0.56
[11]	30,000	10	4	Yes	–0.52
[12]	10,000	6	2	Yes	–0.52
[12]	30,000	6	2	Yes	–0.42
[12]	10,000	10	4	No	–0.48
[13]	59,217	6.2	1	No	–0.57
[13]	46,233	6.2	2	No	–0.60
[14]	23,000	10	2	Yes	–0.52
[15]	30,000	12.6	3	No	–0.55

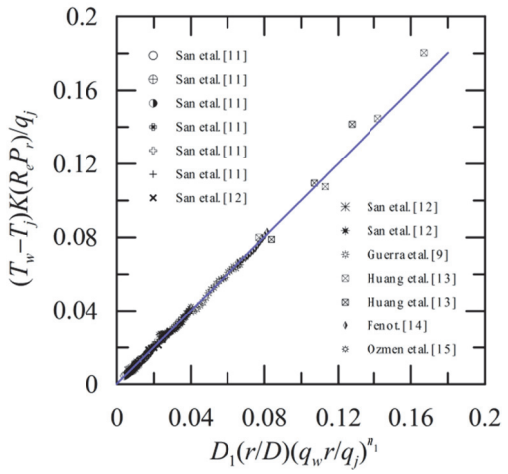

Figure 7 Dependence of T_w with the radial distance.

Figure 7 illustrates the best fitting line applied to the data. The average value of n_1 is –0.52 with a standard deviation of 0.05. Thus, for the implementation of the numerical simulator we have preferred the value $n_1 = -0.5$, which results in $D_1 = 4.34\text{x}10^{-4}$ ($\sigma_{D1} = 6.04\text{x}10^{-4}$). Preferably, the result $D_1 = 5.0\text{x}10^{-4}$ was used in the Simulator.

The heat transfer behaviour of the impinging jet is also analysed through Eq. (11). Figure 8 shows the behaviour of the Nusselt number.

IMPINGING JET SIMULATOR

The numerical simulator was developed in C^{++} in the platform Visual Studio with the MSChart resource. Two versions of the simulator are available, an executable program and an Internet version. Conceived to be run on line, the code has a flexible user's interface to allow access from a microcomputer or even from a cell phone.

The input data are specified in the entrance window. The basic information to be provided by the user is

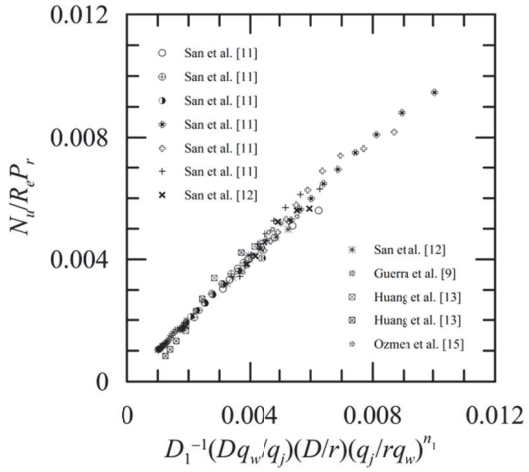

Figure 8 Behaviour of N_u.

- Physical properties of the fluid: ρ, μ, c_p, k.
- Flow geometry: D, H.
- Flow inlet conditions: U_j , T_j .
- Wall heat flux: q_w.

The output of the Simulator shows plots of the radial distributions of U_{max}, y_{max}, τ_w, wall pressure, T_w and T_{min} and local two-dimensional (r, y) velocity and temperature profiles.

The Simulator is based on Eqs. (1) through (15). The results of Poreh et al. [6] are all included in the velocity field analysis.

Once all input data have been assigned, the Simulator runs automatically. The plots are thus automatically updated once every datum is entered. The Simulator is organized to show one plot at a time. In its first version, all plots were shown simultaneously. However, once the number of plots increased to eleven that procedure became very cumbersome.

Two guides are identified in the entrance window, "Fluid Mechanics" and "Heat transfer". Once one is chosen, the desired graph can be displayed by picking the respective guide. The general appearance of the Simulator is shown in Fig. 9.

All data generated by the Simulator can easily be exported to an Excel worksheet by just clicking "Export Datasheet" on the bottom left corner.

FINAL REMARKS

In the course of the present study, about 94 articles were examined for data extraction. In the end, only eleven contained all the necessary information for the validation of Eqs. (1) through (15). These data cover a large range of conditions, thus rendering to the present approach a certain generality.

The present Simulator does not have the ambition of offering a complete picture of the jet impingement phenomenon, but can be used to provide quick answers to many problems of engineering interest, in particular, concerning parameters whose description in literature are difficult to find. The radial distributions of wall shear stress and temperature (at the wall and away from it) characterize some of these cases.

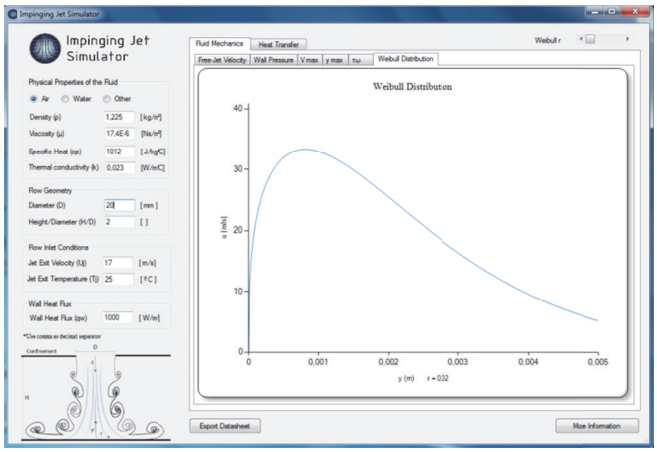

Figure 9 Welcome window of the Simulator.

ACKNOWLEDGEMENTS

In the course of the research, JBRL benefited from a CNPq Research Fellowship (Grant No 301172/2010-2) and from further financial support through Grants CNPq 477354/2011-4 and FAPERJ E-26/102.212/2013. APSF is grateful to the Brazilian National Research Council (CNPq) for the award of a Research Fellowship (Grant No 303982/2009-8). The work was financially supported by CNPq through Grants No 477293/2011-5 and by the Rio de Janeiro Research Foundation (FAPERJ) through Grant E-26/102.937/2011. The authors would like to thank Dr. Fenot for providing us his experimental dataset.

REFERENCES

[1] Sreenivasan, K.R., A unified view of the origin and morphology of the turbulent boundary layer structure. In: *Turbulence Management and Relaminarization*, Eds: H.W. Liepmann and R. Narasimha, 1987.

[2] Narasimha, R., Narayan, K.Y., Pathasarathy, S.P., Parametric analysis of turbulent wall jets in still air, *Aeronautical Journal*, Vol. 77, 1973, pp. 335-339.

[3] Uddin, N., Neumann, S.O., Weigand, B., LES simulations of an impinging jet: on the origin of the second peak in the Nusselt number distribution, *International Journal of Heat and Mass Transfer, Vol.* 57, 2013, pp. 356-368.

[4] Pulat, E., Isman, M.K., Etemoglu, A.B., Can, M., Effect of turbulence models and near-wall modeling approaches on numerical results in impingement heat transfer, *Numerical Heat Transfer*, Part B, 60, 2011, pp. 486-519.

[5] Loureiro, J.B.R. and Silva Freire, A.P., Wall shear stress measurements and parametric analysis of impinging wall jets, *International Journal of Heat and Mass Transfer,* Vol. 55, 2012, 6400-6409.

[6] Poreh, M., Tsuei, Y. G., Cermak, J. E. Investigation of a turbulent radial wall jet, *Trans. ASME: Journal of Applied Mechanics*, Vol. 34, 1967, pp. 457-463.

[7] Fairweather, M., Hargrave, G.K.. Experimental investigation of an axisymmetric, impinging turbulent jet. Part 1: Velocity field, *Experiments in Fluids*, Vol. 33, 2002, pp. 464-471.

[8] Fitzgerald, J.A. Garimella, S.V., A study of the flow field of a confined and submerged impinging jet, *International Journal of Heat and Mass Transfer*, Vol. 41, 1998, pp. 1025-1034.

[9] Guerra, D.R.S. , Su, J., Silva Freire, A.P., The near wall behaviour of an impinging jet, *International Journal of Heat and Mass Transfer*, Vol. 48, 2005, pp. 2829-2840.

[10] Koseoglu, M.F., Baskayab, S., The effect of flow field and turbulence on heat transfer characteristics of confined circular and elliptic impinging jets, *International Journal of Thermal Science* Vol. 47, 2008, pp. 1332-1346.

[11] San, J.Y., Huang, C.H., Shu, M.H., Impingement cooling of a confined circular air jet, *International Journal of Heat and Mass Transfer*, Vol. 40, 1997, pp. 1355-1364.

[12] San, J.Y., Shiao, W. Z., Shu, M.H., Effects of jet plate size and plate spacing on the stagnation Nusselt number for a confined circular air jet impinging on a flat surface, *International Journal of Heat and Mass Transfer*, Vol. 49, 2006, p. 3477-3486.

[13] Huang, L., El-Genk, M. S., Heat transfer of an impinging jet on a flat surface, *International Journal of Heat and Mass Transfer*, Vol. 37, 1994, pp. 1915-1923.

[14] Fenot, M., Vullierme, J.J., Dorignac, E., Local heat transfer due to several configurations of circular air jets impinging on a flat plate with and without semi-confinement, *International Journal of Thermal Science*, Vol. 44, 2005, pp. 665-675.

[15] Ozmen, Y., Baydar, E., Flow structure and heat transfer characteristics of an unconfined impinging air jet at high jet Reynolds numbers, *Heat and Mass Transfer*, Vol. 44, 2008, pp. 1315-1322.

[16] Ozdemir, I.B., Whitelaw, J.H., Impingement of an axisymmetric jet on unheated and heated flat plates, *Journal of Fluid Mechanics*, Vol. 24, 1992, pp. 503-532.

[17] Popiel, C.O., Trass, O., Visualization of a free and impinging round jet, *Experimental Thermal and Fluid Science*, Vol. 4, 1991, pp. 253-264.

[18] Hadziabdi, M., Hanjalic, K., Vortical structures and heat transfer in a round impinging jet, *Journal of Fluid Mechanics*, Vol. 596, 2008, pp. 221-260.

[19] Phares, D.J., Smedley, G.T., Flagan, R., The wall shear stress produced by the normal impingement of a jet on a flat surface, *Journal of Fluid Mechanics*, Vol. 418, 2000, pp. 351-375.

[20] H. Schlichting, *Boundary layer theory*, McGraw Hill, 1979.